

1 **Murine Olfactory Bulb Interneurons Survive Infection with a Neurotropic**  
2 **Coronavirus**

3 D. Lori Wheeler<sup>a</sup>, Jeremiah Athmer<sup>b</sup>, David K. Meyerholz<sup>c</sup>, Stanley Perlman<sup>a,b,#</sup>

4  
5 Interdisciplinary Graduate Program in Immunology<sup>a</sup>, Department of Microbiology and  
6 Immunology<sup>b</sup>, Department of Pathology<sup>c</sup>, University of Iowa, Iowa City, Iowa 52242

7  
8  
9 Running title: Olfactory bulb interneurons survive MHV infection

10 Keywords: Coronavirus, olfactory bulb, encephalitis, interneurons

11  
12 # Address correspondence to Stanley Perlman, M.D., Ph.D., Department of Microbiology and  
13 Immunology, BSB 3-712, University of Iowa, Iowa City, IA 52242; tele: 319-335-8549; FAX  
14 #319-335-9006; email: Stanley-perlman@uiowa.edu

15  
16 Abstract word count: 209

17 Text word count: 3411

18

19 **Abstract.** Viral infection of the central nervous system is complicated by the mostly  
20 irreplaceable nature of neurons, as the loss of neurons has the potential to result in permanent  
21 damage to brain function. However, whether neurons or other cells in the CNS sometimes  
22 survive infection and the effects of infection on neuronal function are largely unknown. To  
23 address this question, we used the rJHM strain (rJ) of mouse hepatitis virus, (MHV), a  
24 neurotropic coronavirus, which causes acute encephalitis in susceptible strains of mice. To  
25 determine whether neurons or other CNS cells survive acute infection with this virulent virus, we  
26 developed a recombinant JHMV that expresses Cre recombinase (rJ-Cre) and infected mice that  
27 universally expressed a silent (floxed) version of tdTomato. Infection of these mice with rJ-Cre  
28 resulted in expression of tdTomato in host cells. The results showed that some cells were able to  
29 survive the infection, as demonstrated by continued tdTomato expression after virus antigen  
30 could no longer be detected. Most notably, interneurons in the olfactory bulb, which are known  
31 to be inhibitory, represented a large fraction of the surviving cells. In conclusion, our results  
32 indicated that some neurons are resistant to virus-mediated cell death and provide a framework  
33 for studying the effects of prior coronavirus infection on neuron function.

34 **Importance.** We developed a novel recombinant virus that allows for the study of cells that  
35 survive an infection by a central nervous system-specific strain of murine coronavirus. Using this  
36 virus, we identified neurons and to a lesser extent, non-neuronal cells in the brain that were  
37 infected during the acute phase of the infection and survived for approximately two weeks until  
38 the mice succumbed to the infection. We focused on neurons and glial cells within the olfactory  
39 bulb because the virus enters the brain at this site. Our results show that interneurons of the  
40 olfactory bulb were the primary cell type able to survive infection. Further, these results indicate

- 41 that this system will be useful for functional and gene expression studies of cells in the brain that  
42 survive acute infection.

43 **INTRODUCTION**

44 Viral upper respiratory infection is a common cause of olfactory dysfunction, in part because the  
45 olfactory epithelium is located adjacent to respiratory epithelium, the site of replication of  
46 multiple viruses that cause upper respiratory tract infection and because olfactory neurons  
47 directly access the environment. Viruses take advantage of this direct connection with the  
48 olfactory bulb (OB) to enter the central nervous system (CNS) (1-6). In the process of gaining  
49 access to the CNS, these viruses damage the olfactory epithelium and the olfactory bulb leading  
50 to altered olfaction (7-11).

51 The process of scent discrimination begins within the olfactory epithelium when  
52 odorants bind odorant receptors on olfactory sensory neurons (OSNs) (12, 13). OSNs project  
53 their axons onto the dendrites of projection neurons (tufted cells and mitral cells) within the  
54 olfactory glomeruli of the OB. These tufted and mitral cells then send axons deeper into the  
55 brain, largely to the primary olfactory cortex but also to secondary and tertiary connections of the  
56 OB. Interneurons within all the layers of the olfactory bulb modulate the signal sent by these  
57 projection neurons. While all olfactory bulb interneurons use gamma-aminobutyric acid as a  
58 neurotransmitter, some also express dopamine. These interneurons, which include granule cells  
59 and periglomerular cells, are characterized by soma size, soma location, dendrite extension, and  
60 expression of calcium-binding proteins (14-17). For example, periglomerular cells have a small  
61 soma, are located in the glomerular layer of the olfactory bulb and express tyrosine hydroxylase,  
62 calbindin, or calretinin. In contrast, granule cells express calretinin but not calbindin or tyrosine  
63 hydroxylase (14, 18, 19). While these interneurons are inhibitory by nature, and anatomical  
64 studies have shown that each subtype extends dendrites, little is known about the function of  
65 these cells or how they are molecularly distinct from each other.

66           Coronaviruses (CoV) are positive-stranded RNA viruses capable of causing disease in a  
67 variety of animals. These diseases range from respiratory, systemic, neurological and  
68 gastrointestinal diseases in domestic, companion and experimental animals to mild and severe  
69 respiratory disease in humans (20, 21). Neurotropic strains of the murine CoV, mouse hepatitis  
70 virus (MHV), cause acute encephalitis and acute and chronic demyelinating diseases of the  
71 central nervous system (22). In specific, the non-recombinant and recombinant (rJ) versions of  
72 neurotropic JHM cause lethal encephalitis. When this virus is intranasally instilled, virus enters  
73 the CNS through the OB by direct infection of OSNs and anterograde transport via the olfactory  
74 nerve. Once in the OB, JHMV spreads trans-neuronally to connections of the main OB (23, 24).  
75 Unlike other neurotropic strains of MHV, JHMV primarily infects neurons (25-28). However,  
76 little is known about the ratio of neuronal to glial infection compared or about the subtypes of  
77 neurons infected by JHMV, although infection of tyrosine hydroxylase-expressing neurons may  
78 be limited to certain regions of the brain (24).

79           The irreplaceable nature of most neurons is a major factor in the long-term morbidity  
80 observed after viral infections of the central nervous system. Loss of individual neurons and the  
81 associated disruption of interconnected neural networks results in permanent damage to the  
82 brain. Though not extensively validated, it would be advantageous for neurons to survive after  
83 viral infection. In support of this, neurons have been shown to survive an attenuated rabies virus  
84 infection (29) but whether this phenomenon occurs with viruses other than attenuated rabies  
85 virus is not known.

86           Here, to study brain cells that survive infection after neurotropic CoV infection, we  
87 developed a recombinant JHM virus that expressed Cre recombinase (Cre). tdTomato mice  
88 contain a transgenic tdTomato cassette in a locus that is universally expressed (*Rosa26* locus)

89 thus allowing for expression of the fluorescent protein tdTomato after Cre-LoxP-mediated  
90 excision of a stop cassette (30). Viral Cre expression within the infected host cell results in  
91 excision of a stop cassette, leading to expression of the red fluorescent protein tdTomato only in  
92 infected cells. Because the host cell contains the tdTomato cassette, cells surviving the infection  
93 permanently express tdTomato even after virus is eliminated. Using this model to assess survival  
94 of neurons after virus clearance, we identified a population of OB interneurons that survive the  
95 infection.

## 96 RESULTS

97 **Construction of a Cre-expressing recombinant JHMV (rJ-Cre).** Although it is established  
98 that rJ infects neurons, including mitral cells (25, 26), it is not known whether any neurons in  
99 general survive this infection, or whether certain neuronal cell types preferentially survive. To  
100 engineer a Cre-expressing rJ virus, we used a previously described system of reverse genetics  
101 utilizing a Bac cDNA clone (pBAC-JHMV<sup>IA</sup>) (31). Cre was inserted into pBAC-JHMV<sup>IA</sup> in  
102 place of ORF4, a gene that is dispensable for viral replication in tissue culture or in mice (32, 33)  
103 using Red recombination with an arabinose-inducible *Flp* recombinase (**Figure 1A**). rJ-Cre was  
104 propagated and analyzed for its ability to replicate in tissue culture cells and to cause lethal  
105 encephalitis in mice. Insertion of the *Cre* gene had little to no effect on virus replication in 17Cl-  
106 1 cells compared to wild-type rJ (**Figure 1B**). Infection of C57Bl/6 mice with  $4 \times 10^4$  rJ-Cre  
107 resulted in morbidity and mortality indistinguishable from that seen in mice infected with rJ  
108 (**Figure 1C**). Together, these results indicate that the insertion of Cre into the rJ genome did not  
109 appreciably alter viral fitness.

110 To assess the functionality of Cre expressed from rJ-Cre, tdTomato mice were intranasally  
111 infected with  $4 \times 10^4$  rJ-Cre. After intranasal infection, rJ accesses the brain by replication in the

112 olfactory receptor neurons and anterograde travel to the neurons of the olfactory bulb. Virus then  
113 spreads transneuronally throughout the brain via primary, secondary and tertiary connections of  
114 the OB, reaching sites in the brainstem, amygdala and midbrain by 7 days post-infection (dpi)  
115 (23, 24). In preliminary experiments, we observed that approximately seven days were required  
116 after inoculation of the animal before tdTomato expression was sufficiently elevated to be  
117 detected by confocal microscopy. By 11 dpi, robust tdTomato levels could be detected by  
118 confocal microscopy in neurons of the olfactory system, including neurons in the brainstem at  
119 sites known to be tertiary connections of the OB (**Figure 2A**). Periglomerular cells (arrows, right  
120 panel) were often degerate (i.e. nuclei were small and hyperchromatic). These changes were  
121 seen on a background of moderate cellular inflammation (**Figure 2B**). These results indicated  
122 that, as expected, rJ-Cre expressed Cre recombinase *in vivo* and expression levels of tdTomato  
123 were sufficient for studying cells that survived the acute infection.

124 **tdTomato-expressing cells remain after virus clearance.** To determine more precisely the  
125 temporal relationship between virus infection and tdTomato positivity, we harvested brains at 4,  
126 7, and 11 dpi and assessed tdTomato and viral nucleocapsid (N)  
127 protein expression using confocal microscopy. In preliminary studies, we noted that tdTomato  
128 expression lagged behind that of viral antigen, likely reflecting the requirement for Cre  
129 expression, transport to the nucleus, DNA excision and mRNA translation before protein can be  
130 expressed. Consequently, we focused our studies on the OB because this is the first site of virus  
131 replication. Further, JHMV and other strains of MHV show a preference for replicating in the  
132 OB even when virus is introduced intracranially, as virus titers are often highest in this part of  
133 the brain (10, 11, 34). After staining OB sections with anti-N MAb at 4 dpi, neither viral antigen  
134 nor tdTomato was detected in the olfactory bulb (**Figure 3A**). However, distinct tdTomato<sup>+</sup> and

135 N protein<sup>+</sup> cells were apparent by 7 dpi. N protein was detected in spite of the increase in auto-  
136 fluorescence seen upon virus infection. At 7 dpi, most tdTomato colocalized with N protein  
137 though some strongly tdTomato<sup>+</sup>, N protein negative cells were clearly visible (**Figure 3B**).  
138 However, by 11 dpi, viral antigen was no longer detected within the OB even as tdTomato  
139 expression became more prominent (**Figure 3A**).

140 As additional support for the notion that the presence of tdTomato<sup>+</sup> cells reflected cell  
141 survival after virus clearance, we measured levels of viral RNA in the OB. Viral subgenomic  
142 RNA within the olfactory bulb was detected at 3 dpi, prior to the detection of virus antigen or  
143 tdTomato positivity and reached peak levels at 5 dpi (**Figure 3C**). Levels of subgenomic RNA  
144 then declined and were detected at low levels at 7 dpi indicating that viral clearance was  
145 occurring. The presence of tdTomato-expressing cells in the OB even as virus was cleared from  
146 this site supports the conclusion that at least a subset of CNS cells was able to clear the infection  
147 and remain viable.

148 **Interneurons of the olfactory bulb survive rJ infection.** As expected, given the cellular  
149 tropism of rJ, most surviving tdTomato-positive cells were neurons as demonstrated  
150 morphologically and confirmed by NeuroTrace staining (**Figure 4**). Some neurons within the  
151 olfactory bulb strongly expressed tdTomato throughout the cell. As demonstrated by  
152 morphology, neurons surviving rJ-Cre infection were largely interneurons (**Figure 4B**); no mitral  
153 cells were tdTomato-positive perhaps indicating that mitral cells did not survive rJ infection.  
154 Surviving interneurons were primarily located in the glomerular cell layer and granule cell layer  
155 of the olfactory bulb (**Figure 5A**). These results indicate that interneurons comprised a large  
156 fraction of cells that survived rJ infection, suggesting an increased ability to survive the viral  
157 infection.



158 Interneurons of the olfactory bulb are classified based on their location and expression of  
159 neurotransmitters and other cell markers. For example, periglomerular interneurons of the  
160 glomerular cell layer can be calretinin, tyrosine hydroxylase or calbindin-positive. To define  
161 more precisely the type of interneuron surviving rJ-Cre infection, we stained olfactory bulbs with  
162 antibodies to tyrosine hydroxylase, calretinin, and parvalbumin. tdTomato-positive cells did not  
163 express any of these markers. While readily detected, tyrosine hydroxylase-expressing cells did  
164 not co-express tdTomato (**Figure 5B**). Similarly, tdTomato<sup>+</sup> parvalbumin<sup>+</sup> and tdTomato<sup>+</sup>  
165 calretinin<sup>+</sup> cells also were not detected (**Figure 5C, D**). These results suggest that expression of  
166 the cell-specific marker was decreased in surviving cells, or alternatively, infection was  
167 predominantly of an interneuron subset not expressing one of the three proteins that we assayed.

168 **Rare glial cells survive rJ infection.** rJ is known to primarily infect neurons (25, 26) and  
169 tdTomato<sup>+</sup> cells were morphologically neurons; however, rJ infection of glia has also been  
170 reported (28, 35, 36). To better characterize the relative proportion of neuronal and nonneuronal  
171 cells in the brain that survive infection, we stained sections from infected tdTomato<sup>+</sup> mice with  
172 antibodies specific for astrocytes and microglia. First, sections were stained with antibody to  
173 glial fibrillary acidic protein (GFAP), a well-described protein expressed by astrocytes. The  
174 results showed that few astrocytes were tdTomato<sup>+</sup> although, a few tdTomato<sup>+</sup> astrocytes were  
175 found (**Figure 6A**). To determine whether microglia survived rJ-Cre infection, we  
176 immunostained OB sections with an antibody to IBA-1, a protein that is upregulated on these  
177 cells at sites of inflammation. Some cells exhibited co-localization of IBA-1 and tdTomato after  
178 infection (**Figure 6B**), but the pattern of co-localization appeared punctate and phenotypically  
179 different from the diffuse tdTomato expression detected in neurons. Therefore, this punctate  
180 pattern may represent microglia/macrophage phagocytosis of tdTomato<sup>+</sup> cells as opposed to *de*

181 *novo* tdTomato expression. Consistent with this interpretation, there was a lack of tdTomato  
182 positivity detected in the nucleus of these cells. To confirm these results, we bred CX3CR1-GFP,  
183 which serve as microglia-reporter mice, to tdTomato mice. F1 progeny from this cross were  
184 infected with rJ-Cre. These mice constitutively express GFP in microglia/macrophages, and will  
185 express tdTomato in cells after viral infection, eliminating the need for immunostaining.  
186 Experiments with CX3CR1<sup>GFP/+</sup> tdTomato<sup>+/-</sup> mice largely recapitulated the punctate IBA1  
187 immunostaining described above. Microglia/macrophages with a punctate pattern of tdTomato  
188 were near tdTomato<sup>+</sup> neurons (**Figure 6C**). However, uncommon cells with the typical  
189 morphology of microglia showing a more diffuse pattern of tdTomato expression in both the  
190 cytoplasm and nucleus were also found, suggestive of rare endogenous infection (**Figure 6C**).  
191 Collectively these results indicate that rJ is capable of infecting glial cells, albeit at low levels,  
192 and that some astrocytes and microglia survive rJ infection. They also suggest, perhaps not  
193 surprisingly, that microglia/macrophages play a role in clearing virus-infected cells.

#### 194 **DISCUSSION**

195 While the consequences of viral infection in the central nervous system can be devastating  
196 because of neuronal loss, little is known about whether neurons that survive are dysfunctional.  
197 The main challenge to studying neurons affected by virus infection is to identify and isolate  
198 those cells after virus has been cleared. Here, we demonstrate a method useful for identifying  
199 previously infected cells by alteration of the host genome using virally-expressed Cre protein.  
200 We used a virulent neurotropic CoV that results in a lethal disease by 12 dpi. We found cells,  
201 especially in the OB, that survived the infection at times when viral antigen could no longer be  
202 detected by immunostaining. These results corroborate previous studies in which populations of  
203 cells that survive infection were identified using Cre-based methodology. In one such study,

204 small numbers of cells, found to be club cells by mRNA sequencing, survived influenza A virus  
205 infection and had increased levels of interferon-stimulated proteins, resulting in an inflammatory  
206 disease (37). In another study, an attenuated Rabies virus-expressing-Cre reporter system showed  
207 that neurons survived up to 6 months after infection. Surviving neurons in this study showed  
208 alterations in transcripts for neuronal function and structure by microarray analysis (29). Our  
209 results using a virulent strain of JHMV indicate that neurons can even survive infection with a  
210 highly pathogenic virus.

211 Our results provide proof of principle for using a Cre-reporter model for studying cells  
212 surviving MHV infection in the central nervous system. Additionally, GFAP and IBA1 staining  
213 confirmed that neurons preferentially survive rJ infection since few astrocytes or microglia  
214 expressed tdTomato after infection. These results are consistent with previous work  
215 demonstrating a tropism for neuronal cells, but it is also possible that glial cells survive infection  
216 less frequently. Future work based on the method described herein will be useful for studying the  
217 CNS of mice infected with CoV with different cellular tropisms. Of particular interest will be the  
218 consequences of infection with the neuroattenuated J2.2-V-1 strain of JHMV, which  
219 preferentially infects oligodendrocytes and causes clinically apparent demyelinating disease. A  
220 Cre-expressing recombinant J2.2 would allow for study of the effects of viral infection on  
221 oligodendrocyte RNA and protein expression and would provide new information on the effects  
222 of prior infection on demyelination and remyelination. Most studies have focused on gross areas  
223 of myelin destruction but such a recombinant virus would facilitate analyses of surviving and  
224 possibly dysfunctional cells.

225 Many viruses replicate in the nasal cavity and the olfactory epithelium, which is distinct  
226 from the respiratory epithelium, and serves as an important portal of virus entry into the CNS (1).

227 Thus, virus is first detected in the OB in experimental infections caused by neurotropic influenza  
228 A virus, West Nile virus and others (2-6). In a similar vein, the OBLV strain of MHV replicates  
229 to high titers in the OB, with little evidence of spread elsewhere in the brains of  
230 immunocompetent mice (10, 11, 34). However, in mice lacking T or B cells OBLV spreads  
231 throughout the brain (34). The propensity for viruses to invade the CNS via the OB, combined  
232 with the uncommonness of viral encephalitis, suggests that the olfactory epithelium, nerve, or  
233 bulb may limit viral spread to and within the CNS, perhaps by modulating the immune response.  
234 Our results indicate that some cells in the OB, especially interneurons, survive the initial virus  
235 infection. These cells are primarily inhibitory and modulate neuronal function. Whether these  
236 surviving neurons have diminished function, resulting in changes in olfaction will require  
237 additional investigation.

## 238 MATERIALS AND METHODS

239 **Cell culture.** MHV-receptor-expressing HeLa cells (HeLa-MHVR), 17Cl-1 cells, and MHV-  
240 receptor expressing BHK cells were grown as previously described (38, 39).

241 **Generation of recombinant JHMV-Cre.** Cre recombinase was cloned into pBAC-JHMV as  
242 previously described (31). Briefly, a PCR product containing Cre-FRT-Kan<sup>r</sup>-FRT and 5' and 3'  
243 homology to the regions just outside ORF4 was created using two-step PCR. A plasmid  
244 containing Cre sequence was a gift from Benjamin tenOever (Icahn School of Medicine). This  
245 cassette was transformed into *E. coli* containing pBAC-JHMV<sup>1A</sup>. Bacteria with successfully  
246 recombined pBAC-JHMV were identified by kanamycin resistance. Correct clones were  
247 amplified and treated with *Flp* recombinase to excise the kanamycin resistance cassette  
248 surrounded by *Flp* recombination targets. pBAC-derived JHMV-Cre was obtained after  
249 transfection as previously described (31). rJ-Cre virus was grown on 17Cl-1 cells, and virus titers

250 were determined on HeLa-MHVR cells (40). 17Cl-1 cells were infected with rJ at a multiplicity  
251 of infection (MOI) of 0.1, and virus from the supernatant and cells was combined prior to  
252 determining viral titers. Virus was passaged five times to obtain sufficient stocks to use in mouse  
253 experiments and an additional three times to assess stability of the Cre insertion. Levels of Cre  
254 expression were unchanged through 7 passages but were diminished by passage 8, indicating  
255 some instability of the Cre gene.

256 **Mice.** Specific-pathogen-free C57Bl/6 mice were purchased from Charles River. B6.Cg-  
257 *Gt(ROSA)26Sor<sup>tm14(CAG-tdTomato)Hze</sup>/J* (tdTomato) mice were purchased from Jackson Laboratories.  
258 B6.129P(Cg)-*Ptprc<sup>a</sup> Cx3cr1<sup>tm1Litt</sup>/LittJ* (CX3CR1-GFP) mice were also purchased from Jackson  
259 Laboratories and bred to tdTomato mice. Mice were maintained in specific-pathogen-free  
260 facilities at The University of Iowa. Male mice were used in all experiments. 5-6-week-old mice  
261 were intranasally inoculated with 40,000 PFU rJHM-Cre after isofluorane anesthesia. After viral  
262 inoculation, mice were observed and weighed daily. To titer virus from infected animals, mice  
263 were sacrificed and perfused with phosphate-buffered saline (PBS). Brain tissue was  
264 homogenized into PBS using a manual homogenizer and frozen. After thawing, cellular debris  
265 was removed by centrifugation, and virus titers in the supernatant were determined on HeLa-  
266 MHVR cells. The University of Iowa Institutional Animal Care and Use Committee approved all  
267 mouse experiments.

268 **RNA analysis.** Olfactory bulbs were collected at indicated times and placed into Trizol (Thermo  
269 Fisher Scientific). RNA was isolated according to the manufacturer's instructions. RNA was  
270 transcribed into cDNA using Moloney murine leukemia virus reverse transcriptase (MMLV RT)  
271 (Thermo Fischer Scientific). Subgenomic RNA levels were measured on a QuantStudio qPCR 3  
272 system (Thermo Fisher Scientific) using previously described subgenomic RNA primers (41).

273 The levels of subgenomic RNA were normalized to hypoxanthine-guanine  
274 phosphoribosyltransferase (HPRT) by the following threshold cycle ( $C_T$ ) equation:  $\Delta C_T = C_T$  of  
275 gene of interest –  $C_T$  of HPRT. All results are shown as a ratio to HPRT calculated as  $2^{-\Delta C_T}$ .

276 **Tissue processing.** After perfusion of the mouse, brains were transferred to 4%  
277 paraformaldehyde solution in a 20:1 volume to weight ratio. After 48 hours, brains were  
278 cryoprotected by immersion in 10% sucrose for 30 minutes, followed by immersion in 20%  
279 sucrose for several hours until brains had dropped to the bottom of the solution. Then, brains  
280 were transferred to 30% sucrose and kept at 4°C overnight. Brains were snap-frozen in tissue  
281 freezing media using a stand-alone Gentle Jane device. 10 or 50  $\mu$ M sections were obtained on a  
282 Thermo cryostat and stored at -80°C. For hematoxylin and eosin staining, brains were removed,  
283 fixed in zinc formalin, then embedded in paraffin. Tissue sections were stained with H&E.

284 **Tissue staining and imaging.** For staining, frozen sections were warmed at room temperature  
285 for 10 minutes. Sections were immersed in PBS for 10 minutes before a 10-minute treatment  
286 with 0.1% Triton-X in PBS. Sections were then rinsed in PBS 3x for 5 minutes each. Next,  
287 samples were incubated in CAS block (Invitrogen) for 10 minutes followed by incubation in  
288 primary antibody diluted in 1% goat serum in PBS overnight at 4°C in a humidity chamber.  
289 Primary antibodies to GFAP (Sigma) at 1:10000, IBA1 (Wako) at 1:2000, parvalbumin (Sigma)  
290 at 1:1000, tyrosine hydroxylase (Millipore) at 1:1000, calretinin (Millipore) at 1:1000 and viral  
291 N protein (kindly provided by Dr. Michael Buchmeier, University of California, Irvine) at  
292 1:10000 were used. Sections were rinsed before incubation with a 1:200 dilution of an  
293 appropriate A488-conjugated goat anti-mouse or anti-rabbit antibody, Thermo Fisher Scientific).  
294 In some cases, Topro-3 (Thermo Fisher Scientific) was included in the secondary antibody  
295 staining solution at a 1:1000 dilution. After rinsing with PBS, slides were mounted with

296 Vectashield anti-fade reagent (Vectashield Laboratories); in some experiments Vectashield  
297 containing DAPI was used. NeuroTrace (Thermo Fisher Scientific) staining was performed  
298 following the manufacturer's protocol. Images were obtained using a Zeiss LSM510 confocal  
299 microscope or an Olympus BX61 light microscope.

300 **Statistics.** Data are presented as mean  $\pm$  SEM unless otherwise indicated. Mann-Whitney *U* tests  
301 were used to analyze differences in means. Log-rank tests were used to determine significant  
302 differences in survival of mice.  $p < 0.05$  were considered significant.

303 **ACKNOWLEDGEMENTS.** We thank Dr. Anthony Fehr and Alan Sariol for critical review of  
304 this manuscript. Supported in part by grants from the NIH (N36592) and National Multiple  
305 Sclerosis Society (RG 5340-A-7). The authors would like to acknowledge use of the University  
306 of Iowa Central Microscopy Research Facility, a core resource supported by the Vice President  
307 for Research & Economic Development, the Holden Comprehensive Cancer Center and the  
308 Carver College of Medicine.

#### 309 REFERENCES

- 310 1. **van Riel D, Verdijk R, Kuiken T.** 2015. The olfactory nerve: a shortcut for influenza  
311 and other viral diseases into the central nervous system. *J Pathol* **235**:277-287.
- 312 2. **Majde JA, Bohnet SG, Ellis GA, Churchill L, Leyva-Grado V, Wu M, Szentirmai E,**  
313 **Rehman A, Krueger JM.** 2007. Detection of mouse-adapted human influenza virus in  
314 the olfactory bulbs of mice within hours after intranasal infection. *J Neurovirol* **13**:399-  
315 409.
- 316 3. **Leyva-Grado VH, Churchill L, Harding J, Krueger JM.** 2010. The olfactory nerve  
317 has a role in the body temperature and brain cytokine responses to influenza virus. *Brain*  
318 *Behav Immun* **24**:281-288.
- 319 4. **Mori I, Nishiyama Y, Yokochi T, Kimura Y.** 2005. Olfactory transmission of  
320 neurotropic viruses. *J Neurovirol* **11**:129-137.
- 321 5. **Faber HK, Gebhardt LP.** 1933. Localizations of the Virus of Poliomyelitis in the  
322 Central Nervous System during the Preparalytic Period, after Intranasal Instillation. *J Exp*  
323 *Med* **57**:933-954.

- 324 6. **Monath TP, Cropp CB, Harrison AK.** 1983. Mode of entry of a neurotropic arbovirus  
325 into the central nervous system. Reinvestigation of an old controversy. *Lab Invest*  
326 **48**:399-410.
- 327 7. **Yamagishi M, Fujiwara M, Nakamura H.** 1994. Olfactory mucosal findings and  
328 clinical course in patients with olfactory disorders following upper respiratory viral  
329 infection. *Rhinology* **32**:113-118.
- 330 8. **Yamagishi M.** 1988. [Immunohistochemical study of the olfactory epithelium in the  
331 process of regeneration]. *Nihon Jibiinkoka Gakkai Kaiho* **91**:730-738.
- 332 9. **Moran DT, Jafek BW, Eller PM, Rowley JC, 3rd.** 1992. Ultrastructural histopathology  
333 of human olfactory dysfunction. *Microsc Res Tech* **23**:103-110.
- 334 10. **Youngentob SL, Schwob JE, Saha S, Manglapus G, Jubelt B.** 2001. Functional  
335 consequences following infection of the olfactory system by intranasal infusion of the  
336 olfactory bulb line variant (OBLV) of mouse hepatitis strain JHM. *Chem Senses* **26**:953-  
337 963.
- 338 11. **Schwob JE, Saha S, Youngentob SL, Jubelt B.** 2001. Intranasal inoculation with the  
339 olfactory bulb line variant of mouse hepatitis virus causes extensive destruction of the  
340 olfactory bulb and accelerated turnover of neurons in the olfactory epithelium of mice.  
341 *Chem Senses* **26**:937-952.
- 342 12. **Murthy VN.** 2011. Olfactory maps in the brain. *Annu Rev Neurosci* **34**:233-258.
- 343 13. **Lodovichi C, Belluscio L.** 2012. Odorant receptors in the formation of the olfactory bulb  
344 circuitry. *Physiology (Bethesda)* **27**:200-212.
- 345 14. **Nagayama S, Homma R, Imamura F.** 2014. Neuronal organization of olfactory bulb  
346 circuits. *Front Neural Circuits* **8**:98.
- 347 15. **Bagley J, LaRocca G, Jimenez DA, Urban NN.** 2007. Adult neurogenesis and specific  
348 replacement of interneuron subtypes in the mouse main olfactory bulb. *BMC Neurosci*  
349 **8**:92.
- 350 16. **Merkle FT, Fuentealba LC, Sanders TA, Magno L, Kessar N, Alvarez-Buylla A.**  
351 2014. Adult neural stem cells in distinct microdomains generate previously unknown  
352 interneuron types. *Nat Neurosci* **17**:207-214.
- 353 17. **Parrish-Aungst S, Shipley MT, Erdelyi F, Szabo G, Puche AC.** 2007. Quantitative  
354 analysis of neuronal diversity in the mouse olfactory bulb. *J Comp Neurol* **501**:825-836.
- 355 18. **Batista-Brito R, Close J, Machold R, Fishell G.** 2008. The distinct temporal origins of  
356 olfactory bulb interneuron subtypes. *J Neurosci* **28**:3966-3975.
- 357 19. **Lledo PM, Merkle FT, Alvarez-Buylla A.** 2008. Origin and function of olfactory bulb  
358 interneuron diversity. *Trends Neurosci* **31**:392-400.
- 359 20. **Perlman S, Netland J.** 2009. Coronaviruses post-SARS: update on replication and  
360 pathogenesis. *Nat Rev Microbiol* **7**:439-450.
- 361 21. **Compton SR, Barthold SW, Smith AL.** 1993. The cellular and molecular pathogenesis  
362 of coronaviruses. *Lab Anim Sci* **43**:15-28.
- 363 22. **Bergmann CC, Lane TE, Stohlman SA.** 2006. Coronavirus infection of the central  
364 nervous system: host-virus stand-off. *Nat Rev Microbiol* **4**:121-132.
- 365 23. **Barnett EM, Perlman S.** 1993. The olfactory nerve and not the trigeminal nerve is the  
366 major site of CNS entry for mouse hepatitis virus, strain JHM. *Virology* **194**:185-191.
- 367 24. **Barnett EM, Cassell MD, Perlman S.** 1993. Two neurotropic viruses, herpes simplex  
368 virus type 1 and mouse hepatitis virus, spread along different neural pathways from the  
369 main olfactory bulb. *Neuroscience* **57**:1007-1025.



- 370 25. **Dubois-Dalcq ME, Doller EW, Haspel MV, Holmes KV.** 1982. Cell tropism and  
371 expression of mouse hepatitis viruses (MHV) in mouse spinal cord cultures. *Virology*  
372 **119**:317-331.
- 373 26. **Knobler RL, Dubois-Dalcq M, Haspel MV, Claysmith AP, Lampert PW, Oldstone**  
374 **MB.** 1981. Selective localization of wild type and mutant mouse hepatitis virus (JHM  
375 strain) antigens in CNS tissue by fluorescence, light and electron microscopy. *J*  
376 *Neuroimmunol* **1**:81-92.
- 377 27. **Knobler RL, Tunison LA, Lampert PW, Oldstone MB.** 1982. Selected mutants of  
378 mouse hepatitis virus type 4 (JHM strain) induce different CNS diseases. Pathobiology of  
379 disease induced by wild type and mutants ts8 and ts15 in BALB/c and SJL/J mice. *Am J*  
380 *Pathol* **109**:157-168.
- 381 28. **Fleming JO, Trousdale MD, el-Zaatari FA, Stohlman SA, Weiner LP.** 1986.  
382 Pathogenicity of antigenic variants of murine coronavirus JHM selected with monoclonal  
383 antibodies. *J Virol* **58**:869-875.
- 384 29. **Gomme EA, Wirblich C, Addya S, Rall GF, Schnell MJ.** 2012. Immune clearance of  
385 attenuated rabies virus results in neuronal survival with altered gene expression. *PLoS*  
386 *Pathog* **8**:e1002971.
- 387 30. **Madisen L, Zwingman TA, Sunkin SM, Oh SW, Zariwala HA, Gu H, Ng LL,**  
388 **Palmiter RD, Hawrylycz MJ, Jones AR, Lein ES, Zeng H.** 2010. A robust and high-  
389 throughput Cre reporting and characterization system for the whole mouse brain. *Nat*  
390 *Neurosci* **13**:133-140.
- 391 31. **Fehr AR, Athmer J, Channappanavar R, Phillips JM, Meyerholz DK, Perlman S.**  
392 2015. The nsp3 macrodomain promotes virulence in mice with coronavirus-induced  
393 encephalitis. *J Virol* **89**:1523-1536.
- 394 32. **Ontiveros E, Kuo L, Masters PS, Perlman S.** 2001. Inactivation of expression of gene  
395 4 of mouse hepatitis virus strain JHM does not affect virulence in the murine CNS.  
396 *Virology* **289**:230-238.
- 397 33. **Ontiveros E, Kuo L, Masters P, Perlman S.** 2001. Analysis of nonessential gene  
398 function in recombinant MHV-JHM. Gene 4 knockout recombinant virus. *Adv Exp Med*  
399 *Biol* **494**:83-89.
- 400 34. **Pearce BD, Hobbs MV, McGraw TS, Buchmeier MJ.** 1994. Cytokine induction during  
401 T-cell-mediated clearance of mouse hepatitis virus from neurons in vivo. *J Virol*  
402 **68**:5483-5495.
- 403 35. **Weiner LP.** 1973. Pathogenesis of demyelination induced by a mouse hepatitis. *Arch*  
404 *Neurol* **28**:298-303.
- 405 36. **Sun N, Perlman S.** 1995. Spread of a neurotropic coronavirus to spinal cord white matter  
406 via neurons and astrocytes. *J Virol* **69**:633-641.
- 407 37. **Heaton NS, Langlois RA, Sachs D, Lim JK, Palese P, tenOever BR.** 2014. Long-term  
408 survival of influenza virus infected club cells drives immunopathology. *J Exp Med*  
409 **211**:1707-1714.
- 410 38. **Yount B, Denison MR, Weiss SR, Baric RS.** 2002. Systematic assembly of a full-length  
411 infectious cDNA of mouse hepatitis virus strain A59. *J Virol* **76**:11065-11078.
- 412 39. **Zhou H, Perlman S.** 2007. Mouse hepatitis virus does not induce Beta interferon  
413 synthesis and does not inhibit its induction by double-stranded RNA. *J Virol* **81**:568-574.

- 414 40. **Pewe L, Zhou H, Netland J, Tangudu C, Olivares H, Shi L, Look D, Gallagher T,**  
415 **Perlman S.** 2005. A severe acute respiratory syndrome-associated coronavirus-specific  
416 protein enhances virulence of an attenuated murine coronavirus. *J Virol* **79**:11335-11342.  
417 41. **Athmer J, Fehr AR, Grunewald M, Smith EC, Denison MR, Perlman S.** 2017. In  
418 Situ Tagged nsp15 Reveals interactions with coronavirus replication/transcription  
419 complex-associated proteins. *MBio* **8**. pii: e02320-16

420

#### 421 **FIGURE LEGENDS**

422 **Figure 1. Characterization of Cre-expressing rJ.** A) Genome of rJ and recombinant rJ  
423 expressing Cre recombinase. B) Replication kinetics of rJ-Cre and rJ. 17CI-1 cells were infected  
424 at an MOI of 0.1 PFU/cell. Virus titers were determined as described in Materials and Methods.  
425 C) Mice were intranasally infected with  $4 \times 10^4$  PFU of the indicated virus and monitored daily  
426 for survival. Data shown are from one experiment representative of two independent experiments  
427 with 5 mice/group.

428 **Figure 2. Visualization of tdTomato-positive cells and brain pathology in brains after**  
429 **rJ.Cre infection.** A) Eleven dpi, brains from Cre-reporter tdTomato mice were harvested,  
430 cryosectioned and imaged without any additional staining. Images are representative of analyses  
431 of 7 mice. B) Histology of olfactory bulbs in naïve and rJ-Cre infected animals at 11 dpi. White  
432 arrow in the inset on the left indicates a healthy periglomerular cell; black arrow in right-sided  
433 inset indicates nuclear changes seen in periglomerular cells. All images are shown at 10X  
434 magnification; insets were cropped to show an individual glomerulus.

435 **Figure 3. Temporal detection of tdTomato and N protein-positive cells.** A) Brains from naïve  
436 and rJ-Cre-infected tdTomato mice were harvested, cryosectioned, and visualized after staining  
437 with a monoclonal antibody to the viral N protein at 4, 7 and 11 dpi. All images are from the  
438 olfactory bulb region. B) Enlargement of boxed area shown in panel A (red arrow indicates  
439 tdTomato<sup>+</sup>N<sup>-</sup> cell while white arrow shows tdTomato<sup>-</sup>N<sup>+</sup> cell; the remainder of the cells are

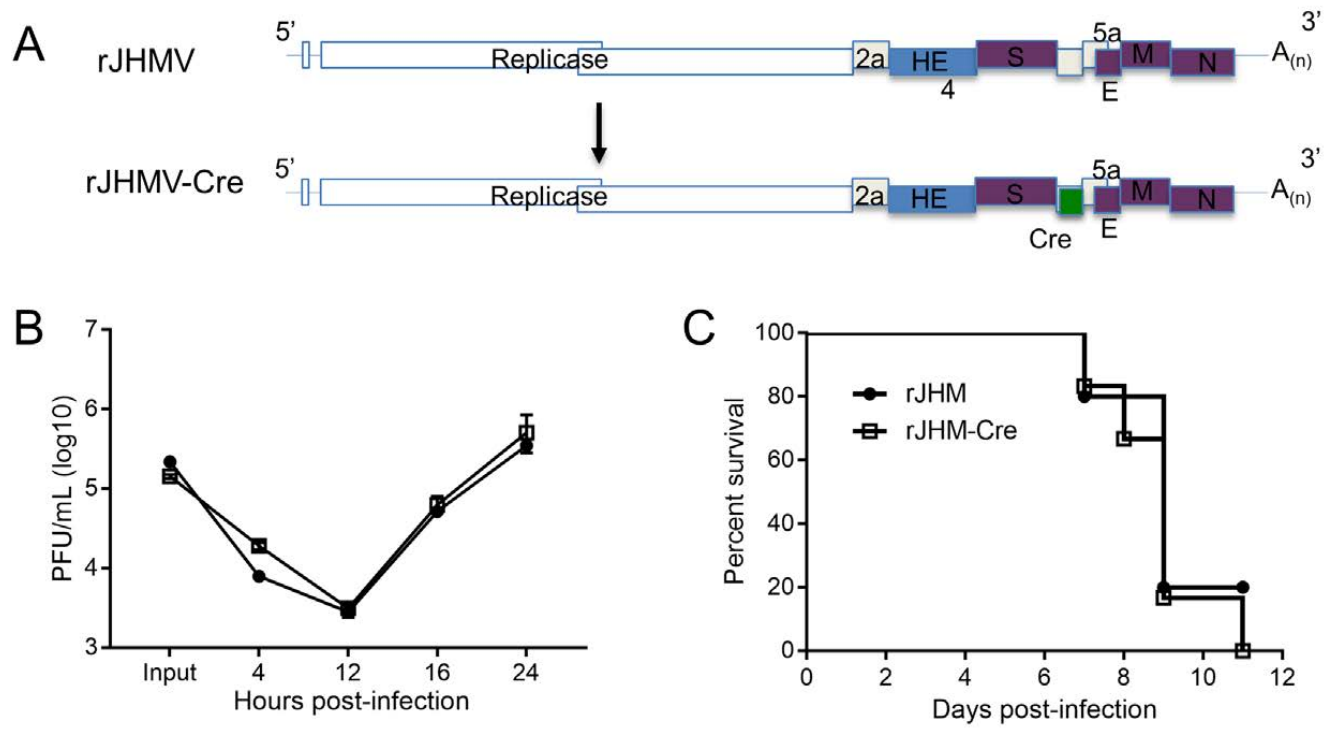
440 positive for both tdTomato and N protein. C) RNA was isolated from the olfactory bulbs of  
441 infected mice at the indicated time points. A quantitative PCR assay was used to determine levels  
442 of sub-genomic viral RNA. Expression of sub-genomic RNA was normalized to HPRT. Data  
443 shown represent 4-5 mice at each timepoint.

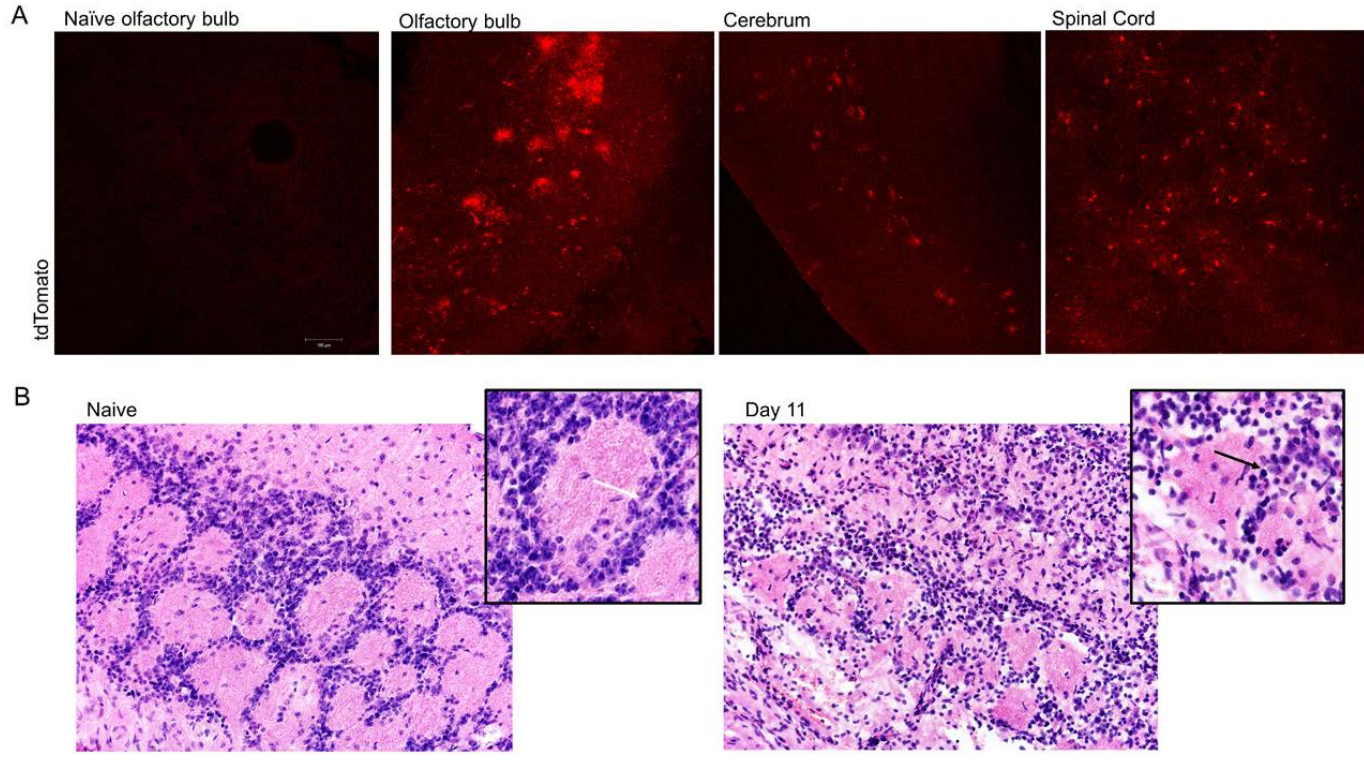
444 **Figure 4. tdTomato-positive cells are largely neurons.** A) rJ-Cre-infected tdTomato mice were  
445 euthanized at 11 dpi. Cryosections from the indicated areas of the brain were stained with the  
446 fluorescent Nissl stain NeuroTrace. B) High-power images of olfactory bulb interneurons stained  
447 with NeuroTrace. Images are representative of 3-5 mice.

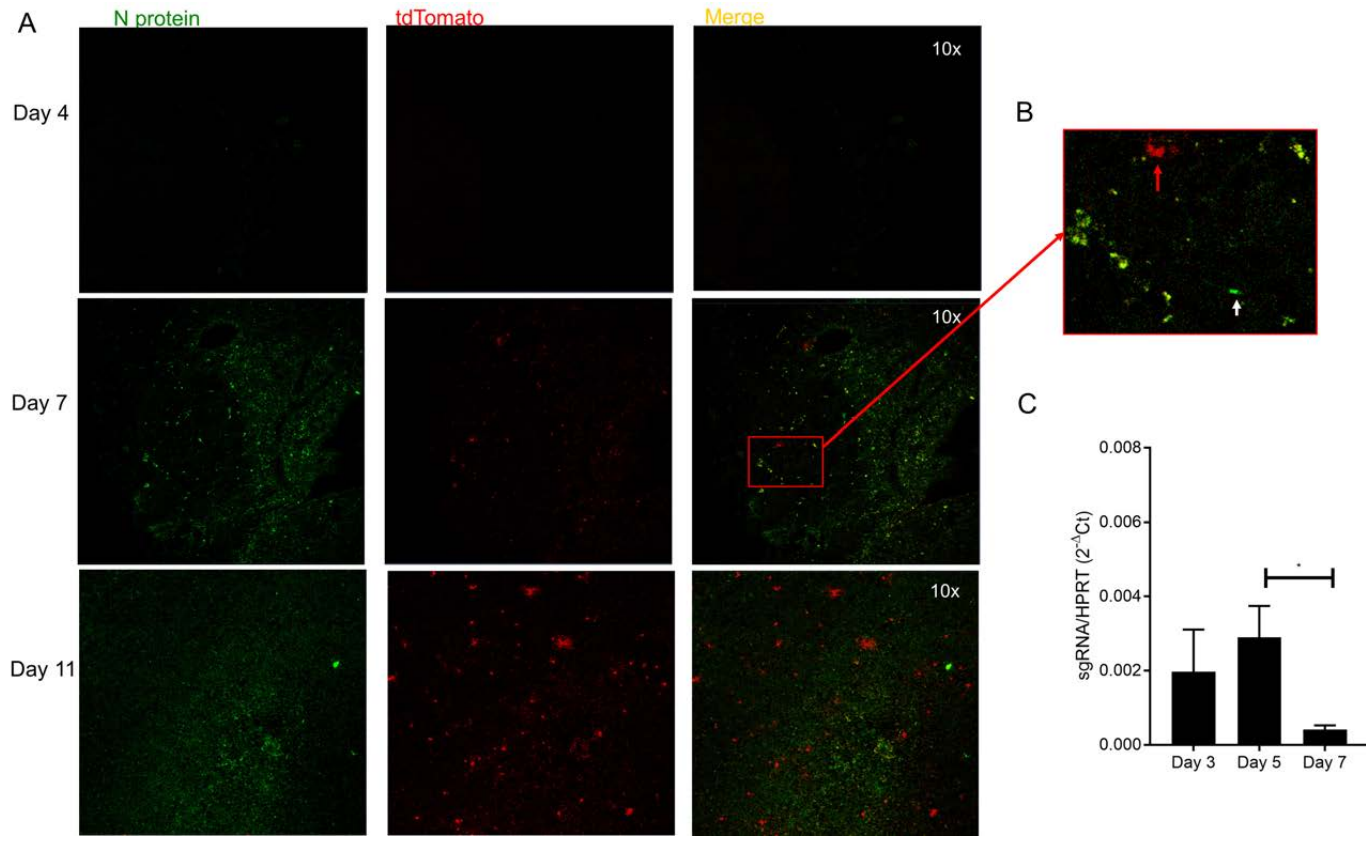
448 **Figure 5. Surviving tdTomato-positive cells in the OB are primarily interneurons.** rJ-  
449 Cre-infected brains were harvested, cryosectioned and stained as indicated. A) Low-power view  
450 of the olfactory bulb showing the anatomical location of surviving tdTomato-positive cells. The  
451 glomerular layer (GL) and granule cell layer (GCL) are labeled. B-D) Tyrosine hydroxylase (B),  
452 Parvalbumin (C), and Calretinin (D) antibody staining of cryosectioned olfactory bulbs. All  
453 images are from the olfactory bulb region at 11 dpi and are representative of 3-5 mice.

454 **Figure 6. A small fraction of glia is tdTomato-positive.** Brains from rJ-Cre infected tdTomato  
455 mice were harvested at 11 dpi, cryosectioned and stained with antibodies to detect astrocytes (A,  
456 GFAP) or microglia (IBA1, B). C) Brains from tdTomato<sup>+/-</sup> CX3CR1<sup>GFP/+</sup> mice were harvested at  
457 11 dpi, cryosectioned and visualized after Topro-3 nuclear staining. White arrows indicate  
458 surviving, double-labeled cells (A, B, and C). Yellow arrows in panel C indicate punctate  
459 tdTomato, CX3CR1-GFP double-labeling.

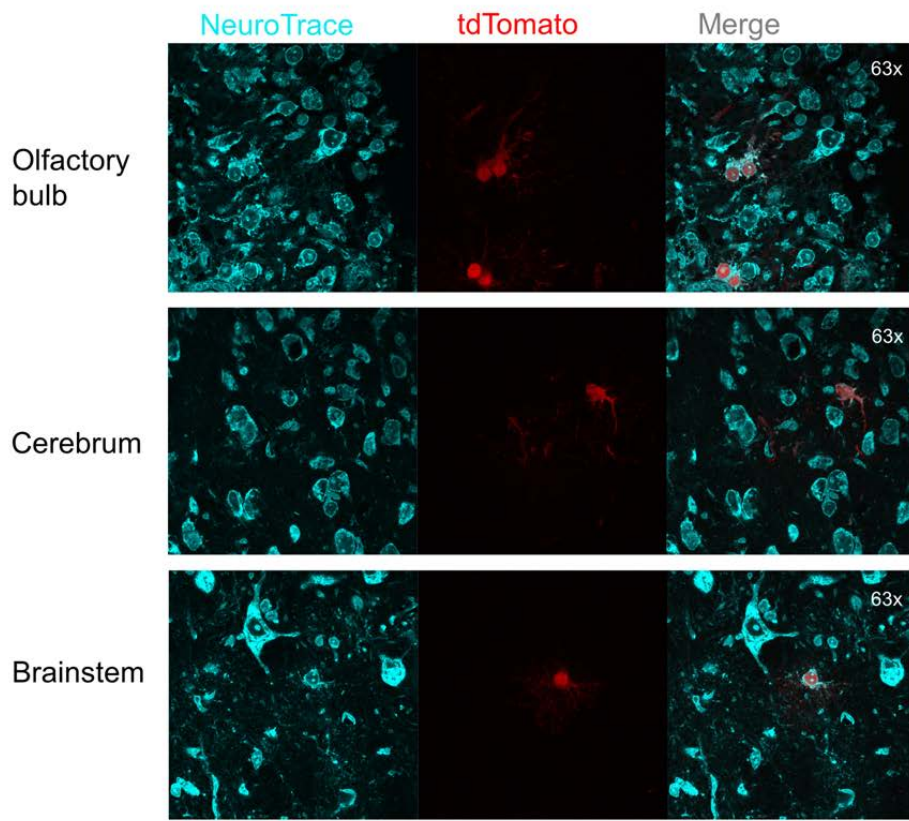
460







A



B

